Bioactive Materials 3 (2018) 225–235

Contents lists available at ScienceDirect

Bioactive Materials

journal homepage: http://www.keaipublishing.com/en/journals/bioactive-materials/

Fabrication and characterization of biodegradable Mg-Zn-Y-Nd-Ag alloy: Microstructure, mechanical properties, corrosion behavior and antibacterial activities

Yashan Feng, Shijie Zhu, Liguo Wang, Lei Chang, Yachen Hou, Shaokang Guan*

School of Materials Science and Engineering, Zhengzhou University, Zhengzhou, 450002, China

ARTICLE INFO

Article history:
Received 20 November 2017
Received in revised form
29 January 2018
Accepted 1 February 2018
Available online 3 April 2018

Keywords:
Magnesium alloy
Silver
Antibacterial
Corrosion resistance

ABSTRACT

Magnesium (Mg), a potential biodegradable material, has drawn wide attention in the bone reconstruction field. However, Mg alloys, served as the bone graft substitution, remain a clinical challenge, the antibacterial activity of which is required to be enhanced. Here, we prepared biodegradable magnesium Mg-Zn-Y-Nd-Ag and then had it been further densified by extruding. The microstructure evolution of the as-cast and as-extruded Mg- Zn-Y-Nd-Ag was characterized using optical microscope and X-ray diffraction analyses (XRD). The results showed that the microstructure of the as-cast alloys was mainly dendrites, between which, the second phase was mainly distributed; with the increase of Ag additions, grain structure was further refined as well as the increase of amount of the second phase. After the extrusion, the grains were further refined. Microhardness tests indicated that both of the increase of Ag content and the extrusion process improved the microhardness of the alloys, specially the later. A systematic investigation of the in vivo antibacterial capability of *Staphylococcus aurous* and *Escherichia coli* was performed, and the results of which indicated that all Mg-Zn-Y-N-xAg (x = 0.2, 0.4, 0.6, 0.8) alloys exhibited certain antibacterial property, which would increased with the increase of Ag content. Taken all together, the antimicrobial property of the as-extruded alloy containing 0.4 wt% Ag exhibited the relatively better antimicrobial properties and mechanical property with the relatively small loss in corrosion resistance, which suggested the potential utility of as-extruded Mg-Zn-Y-N-0.4Ag in treating orthopedic infections.

1. Introduction

Nowadays, magnesium alloy, which is in possession of good biodegradability and high load capacity, has become a research hotspot in researches, drawing wide attention in researches on biological materials, specially the repair of bone fracture [1–4]. However, the lack of antibacterial property of the bone graft substitution often results in postoperative infection and loss of bone tissue, which needs follow-up treatment, and sometimes the severe infection even lead to a second operation [5]. To reduce such kind of the postoperative infection, the functionalization of antimicrobial property of Mg alloy substrate has been targeted in many publications [6,7] (see Table 1).

Mg alloys with antibacterial property have been produced by means of adding antibacterial alloying element. For instances, Hui Qin et al. has fabricated Mg-Nd-Zn-Zr by alloying with neodymium (Nd), zinc (Zn), zirconium (Zr), as the consequence, the novel Mg alloy produced with proper addition of the elements exhibited better biocompatibility and antimicrobial properties [8]. Yang Li et al. prepared biodegradable magnesium-copper alloys with various Cu contents, among which the alloy containing 0.25 wt% Cu exhibited the highest antibacterial activity and favorable biocompatibility, on basis of the assessment on their potentiality for treating methicillin-resistant *Staphylococcus aureus*-induced osteomyelitis [6]. Compared with other elements, silver (Ag) has the strong anti-microbial ability, which could kills off germs at relatively lower concentrations [9]. Ag has attracted great attention as an effective biocide against wide range of microorganisms that enables the Ag with capability to reduce many bacterial infections

* Corresponding author.
E-mail address: skguan@zzu.edu.cn (S. Guan).
Peer review under responsibility of KeAi Communications Co., Ltd.

https://doi.org/10.1016/j.bioactmat.2018.02.002

Table 1
The concentration of bacteria after co-culture with Mg-Zn-Y-Nd-xAg for 24 h.

Samples	Blank control	Mg-Zn-Y-Nd	Mg-Zn-Y-Nd-0.2Ag	Mg-Zn-Y-Nd-0.4Ag	Mg-Zn-Y-Nd-0.6Ag	Mg-Zn-Y-Nd-0.8Ag
S. aureus	2.72×10^{14}	1.76×10^{12}	6.50×10^{10}	3.20×10^{10}	2.40×10^{10}	7.10×10^{9}
E. coli	1.63×10^{12}	1.15×10^{11}	5.50×10^{8}	2.90×10^{8}	2.80×10^{8}	9.00×10^{7}

in a long duration [10]. Thus, alloys doped with silver have been clinically applied in dentistry, implantation and wound healing. Chiung-Fang Huang et al. prepared Ag-containing AISI 316L that exhibited excellent antibacterial properties against both *Staphylococcus aureus* and *Escherichia coli*, when the content of Ag is $\geq$ 0.2 wt% [11]. Y.F. Zheng fabricated TiNiAg ternary alloy by using the arcmelting method, which had higher strength and possess similar corrosion resistance and cyto-biocompatibility compared with TiNi binary alloy. Moreover, TiNiAg alloy also show good antimicrobial properties [12]. Kuo-Hsing Liao et al. found that when it contains about 0.3 wt% Ag, the alloy would exhibit excellent antibacterial property against *E. coli,* along with an AR up to nearly 100%.

The purpose of this work is to test the feasibility of introducing the antibacterial function to Mg-Zn-Y-Nd by the effective addition of alloying element Ag [13]. Some characterizations (metallographic test, mechanical testing, corrosion resistant test, antibacterial activity), had been carried out in order to fully characterize the individual individuate analogies and differences of Mg-Zn-Y-Nd alloy that doped with different Ag content.

2. Materials and methods

2.1. Specimen preparation

Mg-Zn-Y-Nd-xAg (x = 0.2, 0.4, 0.6, 0.8) alloys were prepared by melting pure Mg (99.9 wt%), Pure Zn (99.9 wt%), Mg-30 wt% Y, Mg-30 wt% Nd, pure Ag (99.9 wt%) in an electrical resistance furnace. After all the alloying element were placed in the crucible, the crucible was heated to and kept at the temperature of 720 °C and kept for 20 min. All processes of the mixing, melting, and casting processing were performed under protective atmosphere (CO_2 and SF_6). After homogenizing annealing, the alloy ingot was then further extruded into a rod with a diameter of 20 mm at the temperature of 320 °C and with an extrusion ratio of 1–4 m/min.

2.2. Microstructure characterization

An optical microscope (leica DM4000M, Germany) was used to examine the microstructure of the specimen. Before the determination, both the as-cast and as-extruded samples were firstly grounded with SiC papers to 1200 grid, and then the alloys were etched with nitric acid and picric acid, respectively; afterward, the treated samples were rinsed with deionized water, and then dried in air. The crystalline phase of the as-cast and as-extruded Mg-Zn-Y-Nd-xAg alloys were identified with X-ray diffractometer (XRD philips 1700X, philips, Netherlands) using Cu Kα1 radiation (at a scan rate of 4°/min).

2.3. Microhardness test

The microhardness test was carried out on a HX-10007M/LCD microhardness tester with an applied load of 0.98 N and a loading time of 15 s. The final results were the average value of at least 5 independent measurements.

2.4. Electrochemical studies

The corrosion behaviors of the alloys were studied by potentiodynamic polarization and electrochemical impedance spectroscopy (EIS), using a classical three electrodes cell that comprised an auxiliary electrode of platinum rod, a reference electrode of saturated calomel electrode, and a working electrode of the samples. The electrolyte was simulated body fluid (SBF) [14] and maintained at 37 °C, and the sample area was embedded into resin with a 1 cm^2 area being exposed to the solution. Prior to measurement, the sample was kept in the solution for 30 min. The potentiodynamic polarization tests were carried out at a scan rate of 0.5 mV/s using an electrochemical station; while, the impedance measurements were carried out under a 10 mV root-mean-square perturbation from 100 kHz to 10 mHz.

2.5. Immersion test

For immersion tests, each sample was carefully embedded into silica gel with only one side of 1 cm^2 being exposed. Then samples were immersed in 20 ml SBF in a sterilized bottle in a water bath at 37 °C for 3 days. For hydrogen evolution test, the quantity of hydrogen evolution was recorded at specified time points. The morphology of the samples after immersion was analyzed using scanning electron microscope (SEM Quanta-200, FEI, Netherlands) equipped with EDS (energy dispersive X-ray spectroscopy) after spray-gold treatment.

2.6. Antibacterial evaluation

Before antibacterial experiment, stainless steel portable sterilizer (DSX-280B type, Shanghai Shenan Medical Instrument Factory, China) was used to sterilize the sample under conditions of sterilization temperature at 121 °C, pressure of 1 atm, and sterilization time of 20 min. The experimental strains involved were *Escherichia coli* and *Staphylococcus aureus* and the experimental method applied was referenced to GBT 16886.12–2005 [21]. Firstly, the Mg-Nd-Zn-Zr-xAg alloys (x = 0, 0.2, 0.4, 0.6, 0.8) were respectively placed in a prepared broth medium inoculated with bacterial solution, and the concentration of the bacteria at the time was measured. After the co-cultured for 24 h, the bacterial solution was diluted by 10^{12}–10^{2} and continuously inoculated in agar medium. Afterward the number of bacteria in the incubator was recorded after 24 h and then the antibacterial rate was calculated. In order to investigate the antibacterial properties of the Mg-Zn-Y-Nd-Ag and Mg-Zn-Y-Nd-0.2Ag alloys with an extended cultured time, the time points for recording the number of bacteria number were set as and practically conducted at 0 h, 2 h, 4 h, 8 h, 24 h, 48 h, 72 h, respectively.

3. Results and discussion

3.1. Microstructures and phase composition of as-cast Mg-Zn-Y-Nd-xAg alloys

The microstructures of the as-cast Mg-Zn-Y-Nd-xAg alloys are shown in Fig. 1. From which, it is seen that the white block phase, the dark phase and the thin plate-like phases (second-phase

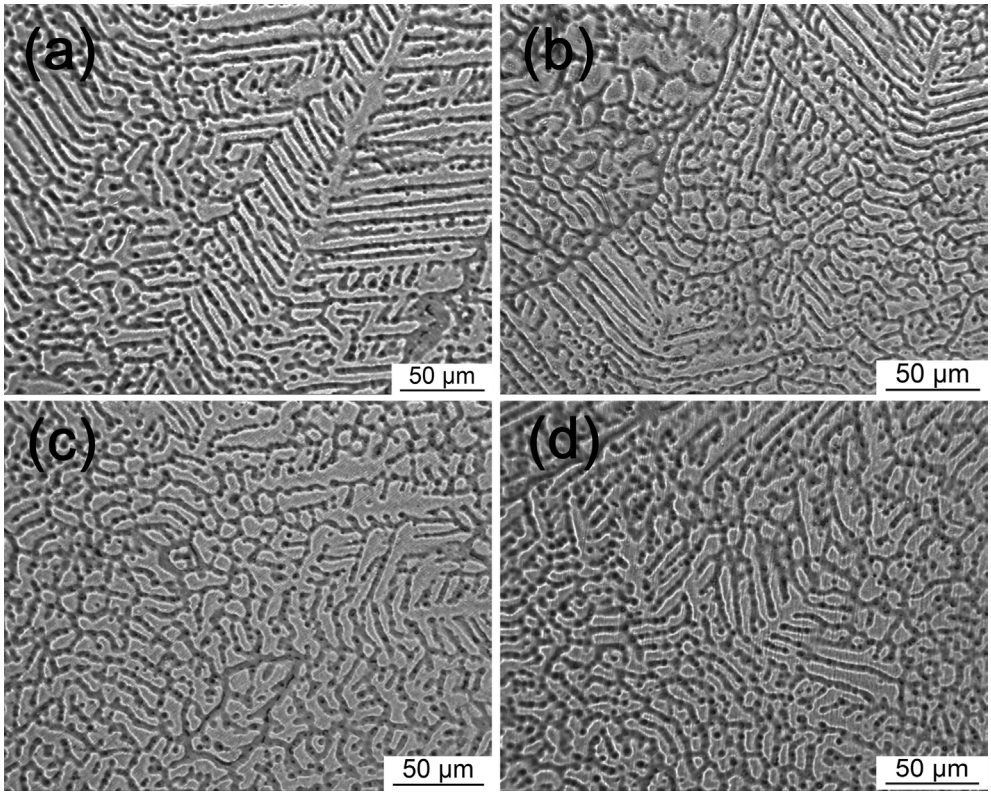

Fig. 1.

particle) exist in all alloys. These microstructures can be mainly regarded as coarse dendrites and secondary dendrites. Second-phase particles chiefly distribute in area between grain boundary and dendritic arm. The size of dendrites become more refined with the increases of Ag content, and the second dendrite arm spacing (SDAS) is decreased from 10 μm to 8 μm as well. Both dendrites and secondary dendrites are relatively coarse and the spherical second phase is mainly and dispersively distributed among dendrites in the alloy with the Ag content of 0.2 wt%; With increase of the Ag content to 0.4 wt% and 0.6 wt%, dendrites are more refined and the distribution of second phase are more dispersive in the matrix. While, when the content of Ag is further increased to a value of 0.8 wt %, the structure of the alloy became more uniform and own maximum number of spherical second phase that uniformly dispersed in matrix.

Casting solidification process pertains to non-equilibrium solidification as the metal model was cooled quickly, which leaded to heterogeneous diffusion of atomics. Thus, there are significant differences in the orientation and size of dendrites with mainly coarse dendrites in alloy microstructure. Part of Ag was dissolved into Mg matrix, and remaining part was combine with other elements to form second-phase, which retarded the growth of (Mg) matrix and refine dendrites.

The XRD diffraction patterns of the as-cast Mg-Zn-Y-Nd-xAg alloys are presented in Fig. 2. There are three kinds of diffraction peaks, which correspond to $MgZn_2$, X-phase ($Mg_{12}YZn$) and $Ag_{51}Nd_{14}$ phases detected as the second phase of the alloys. $Ag_{51}Nd_{14}$ phases could be identified out in all alloys with different Ag content. It is well known that the larger the electronegativity they have, the easier it is to form a second phase. Compared to electronegativity difference of each element with Ag element, the Nd has the largest electronegativity with value of 0.79, followed by Y (0.71) and Mg (0.62). Thus, Ag element was preferentially combined with Nd element and formed $Ag_{51}Nd_{14}$.

3.2. The microstructure and phase composition of extruded Mg-Zn-Y-Nd-xAg alloys

The optical micrographs of the extruded Mg-Zn-Y-Nd-xAg alloys can be seen in Fig. 3. It is stated from the figure that the phases of the alloys were refined after extrusion process compared with the as-cast alloys. The breakdown of coarse dendrites along with dynamic recovery and recrystallization were occurred during extrusion process, which may change the coarse dendrites into equiaxed grains in alloys. The grain size decrease from 15 μm to 2.2 μm with the increase of Ag content from 0.2 wt% to 0.8 wt% in the alloy. The coarse second phase in as-cast alloys are mainly distributed along the grain boundary and dendrite arm in Fig. 1. However, the relatively few second-phases distributed like spots in extruded alloy is because of higher temperature and pressure during extrusion process, which caused the dissolution of second-phase dissolved in matrix or conversion into equiaxed grains. As can be seen from the above analysis, the micro structure of as-cast alloys is mainly of dendrites with second phase distributed dispersively. However, the coarse particle goes against properties of mechanics and corrosion resistance [15], so the treatment of extrusion process to alloys may provide a good performance of the mechanics and corrosion resistance.

Fig. 4 is the XRD diffraction patterns of extruded Mg-Zn-Y-Nd-xAg ($x = 0.2, 0.4, 0.6, 0.8$) alloys, which shows that the phases of alloys were changed after extrusion process compared with as-cast alloys. It is apparent that the Mg-Zn-Y-Nd-0.8Ag extruded alloy is composed of two main phases, MgZn and $Mg_{24}Y_5$, while $Mg_{24}Y_5$ and Mg_2Zn_{11} are detected in other extruded alloys. The second phase of $Ag_{51}Nd_{14}$ is undetected in extruded alloys compared with that of as-cast alloy, which is attributed to the dissolution of a large portion of second phases into the matrix after homogenization

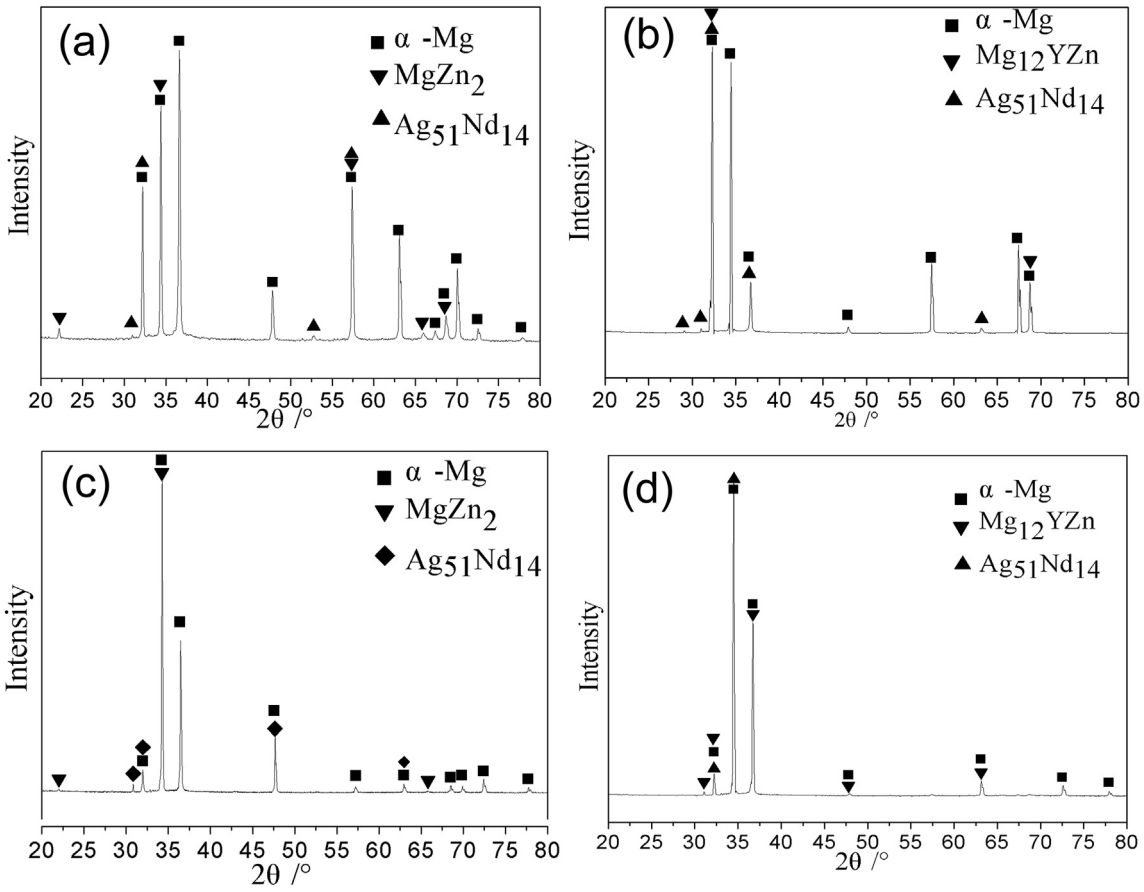
(a)
α -Mg
MgZn2
Ag51Nd14
Intensity
2θ /°
(b)
α -Mg
Mg12YZn
Ag51Nd14
Intensity
2θ /°
(c)
α -Mg
MgZn2
Ag51Nd14
Intensity
2θ /°
(d)
α -Mg
Mg12YZn
Ag51Nd14
Intensity
2θ /°

Fig. 2.

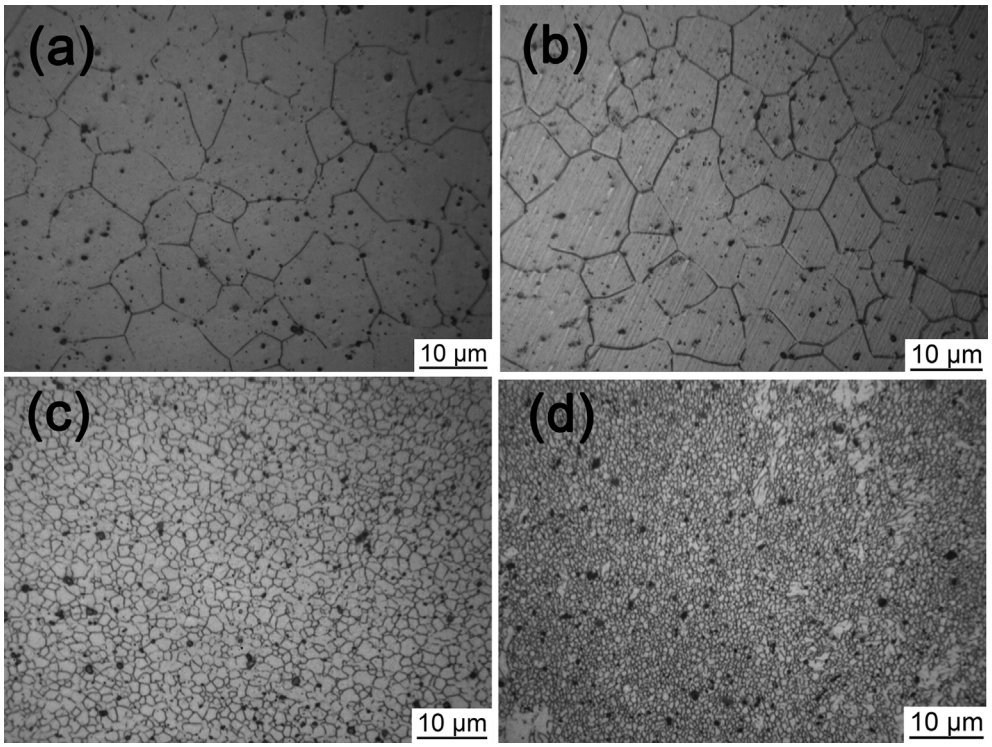
(a)
10 μm
(b)
10 μm
(c)
10 μm
(d)
10 μm

Fig. 3.

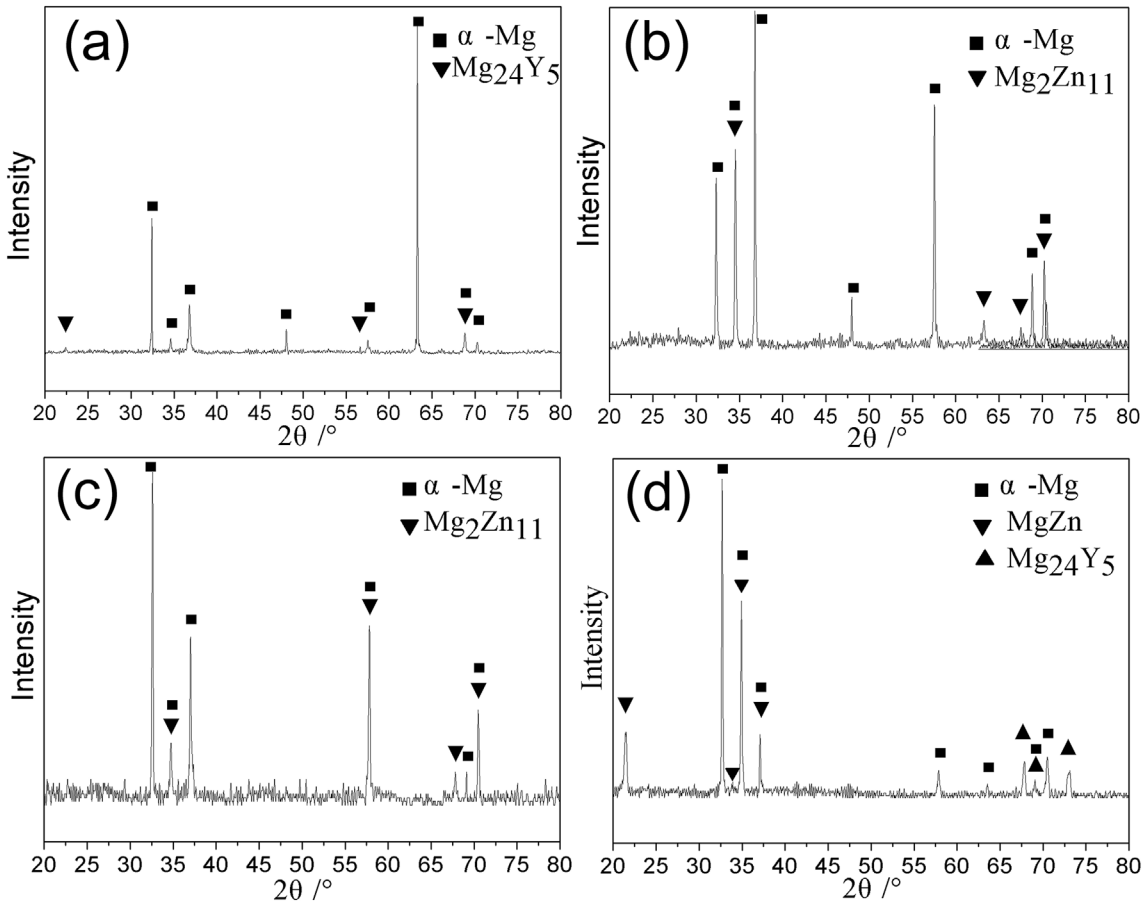

Fig. 4.

treatment and extrusion process.

3.3. The microhardness of Mg-Zn-Y-Nd-xAg alloys

Vickers microhardness test was applied to reflects the ability to resist plastic deformation of metal surface. A new study indicates that the microhardness of the alloys can be enhanced obviously with the addition of Ag [16].

The values of as-cast and as-extruded Mg-Zn-Y-Nd-xAg alloys as determined by microhardness are shown in Fig. 5, illustrating that the average hardness value of as-cast Mg-Zn-Y-Nd-xAg (x = 0, 0.2, 04, 0.6, 0.8) alloys are 48 HV, 50.3 HV, 50 HV, 55.6 HV and 51.2 HV, respectively. As is shown in Fig. 5, the average microhardness value of the alloys is consistently increased until the Ag content of about 0.6% was attained and then slightly declined after then at 0.8 wt%, which is however still significantly higher than the peak hardness of Mg-Zn-Y-Nd alloys. Such behavior is attributed to refined dendrites and more uniform microstructure that generated after adding Ag element that owns strong solid-solution effect. Compared with the as-cast Mg-Zn-Y-Nd-xAg, the microhardness of extruded Mg-Zn-Y-Nd-xAg alloys is obviously improved, which is because the deformation process obviously refined the grain. During manufacturing processes, the grains are broken and the size of which are decreased with further heterogeneous diffusion.

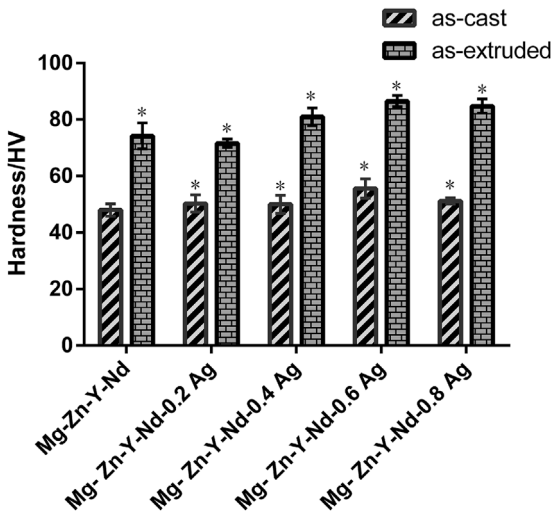

Fig. 5.

3.4. Corrosion resistance

3.4.1. Electrochemical test and hydrogen evolution test

The hydrogen evolution curves of the as-cast and as-extruded Mg-Zn-Y-Nd-xAg (x = 0.2, 0.4, 0.6, 0.8) are shown in Fig. 6. From the figure, it is clearly indicated that the hydrogen evolution quantity of both as-cast and as-extruded Mg-Zn-Y-Nd-xAg materials in SBF is gradually increased with the time extension, and the hydrogen emitted from alloys was gradually accelerated with the increasing content of silver in alloys. In comparison to the as-cast alloys, the hydrogen evolution quantity of as-extruded alloys was

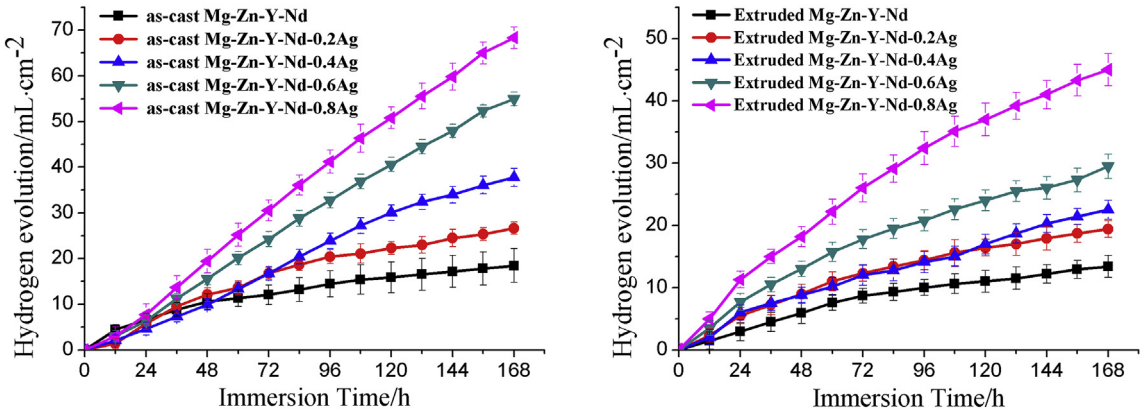

Fig. 6.

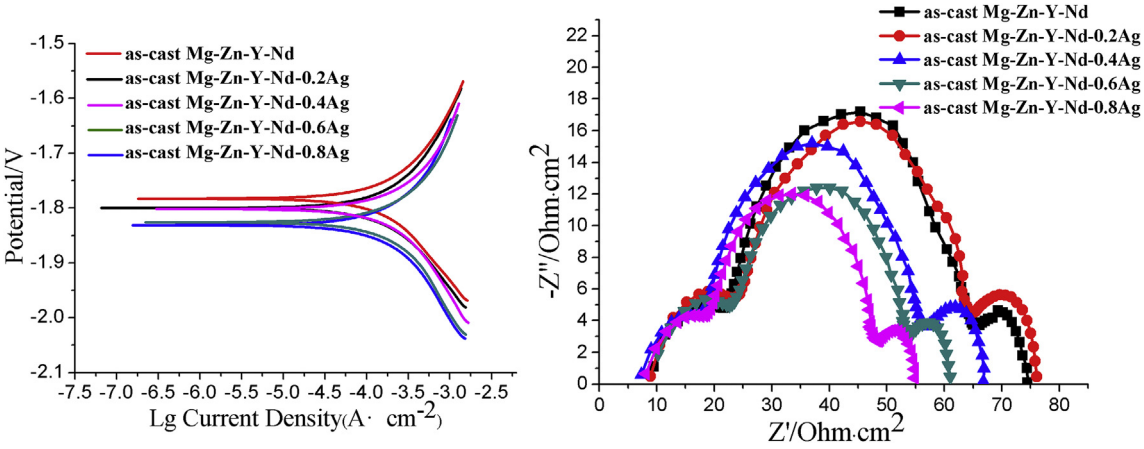

Fig. 7.

relatively lower. Fig. 7 shows the potentiodynamic polarization curves and EIS of the as-cast Mg-Zn-Y-Nd and its alloys with different Ag content. From the potentiodynamic polarization curve, the self-corrosion potential of the Mg-Zn-Y-Nd-xAg shows a decreasing trend with the increase of Ag content. As is shown in Fig. 7, the high-frequency capacitive loop in EIS indicates the capacity of charge transfer, whereas the inductive loop can be attributed to the dissolution and pitting corrosion of Mg [22]. It is evident that the corrosion resistance is clearly decreased due to the smaller dimensions of the capacitive loops. In addition, the capacity of charge was gradually increased with the increase of the Ag content, indicating the gradual decreasing corrosion resistance. Fig. 8 shows the electrochemical results of the as-extruded Mg-Zn-Y-Nd and its alloys with different silver content. As is shown in Fig. 8, the corrosion resistance of extruded alloys still declines with the increasing composition of silver, however, it is absolutely higher

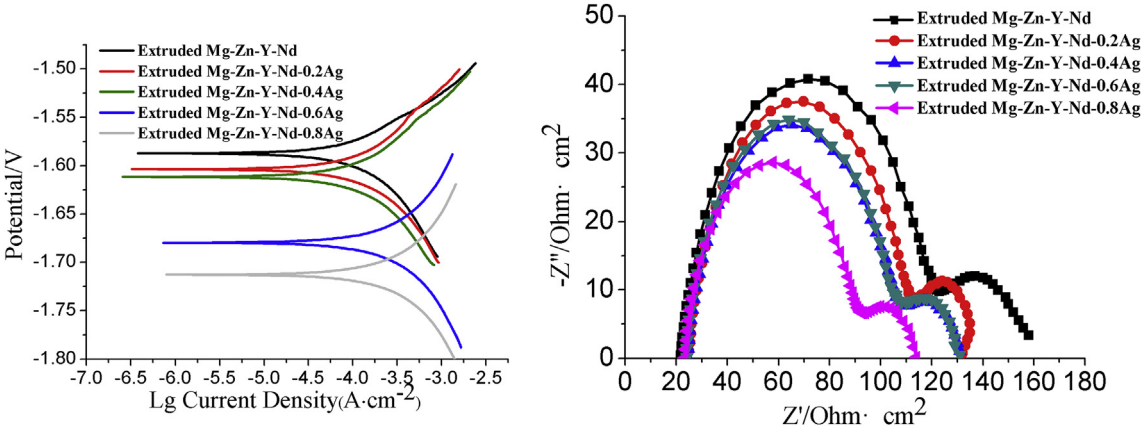

Fig. 8.

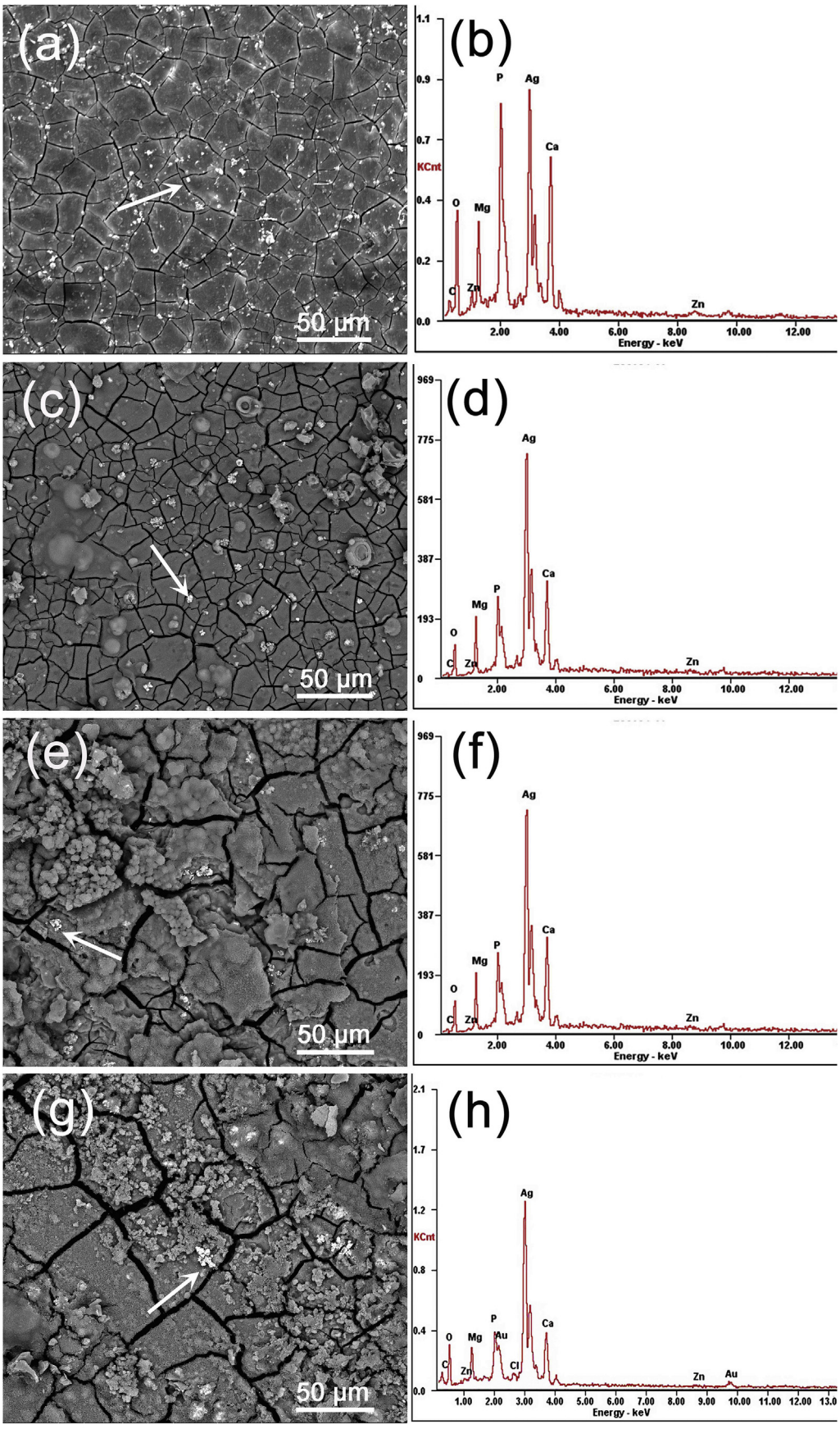
(a)
50 μm
(b)
KCnt
O
Mg
P
Ag
Ca
Zn
Energy - keV
(c)
50 μm
(d)
(e)
50 μm
(f)
(g)
50 μm
(h)
Au
Cl

Fig. 9.

than that of the original as-cast Mg-Zn-Y-Nd alloy, especially for the Mg-Zn-Y-Nd-0.2Ag and Mg-Zn-Y-Nd-0.4Ag. Comparatively analyzing with respect to production rate of hydrogen and polarization curves of the as-cast and as-extruded alloys, the results suggested that the two are different in corrosion resistance in certain degree. This is mainly due to an inhomogeneous structure of as-cast alloys and consequences of distribution of second phase in alloys, including formation of bigger corrosion pits during corrosion process, enlargement of contact areas between alloys and simulated body fluid and acceleration of the corrosion rate. Because of the extrusion process of alloys, dendrites were eliminated, grains become obviously finer, and structures appear more homogeneous. Moreover, from analysis of the XRD of extruded Mg-Zn-Y-Nd-xAg (Fig. 4), silver is almost not found in second phase. Therefore, through homogenization and extrusion processes, silver in alloys tends to dissolves into the matrix, which attenuates the effects of second phase silver ($Ag_{51}Nd_{14}$ and $Mg_{54}Ag_{17}$) on alloys corrosion resistance. As a result, the corrosion resistance of extruded alloys is apparently better than that of cast alloys.

3.4.2. Immersion test

By the analysis and discussions above, the as-extruded alloys exhibited the better mechanical property and corrosion resistance compared with as-cast alloys, thus the corrosion morphology of the as-extruded Mg-Zn-Y-Nd-xAg alloys is to be discussed as the following.

Fig. 9 shows the corrosion morphology analysis of as-extruded Mg-Zn-Y-Nd-xAg ($x = 0.2, 0.4, 0.6, 0.8$) alloys in SBF for 72 h. Varying degrees of crack alloys surfaces are observed, which due to the stress difference when losing water during the drying process. In Fig. 9, the crack of Mg-Zn-Y-Nd-0.2Ag and Mg-Zn-Y-Nd-0.4Ag alloy is relatively slight, and Mg-Zn-Y-Nd-0.6Ag and Mg-Zn-Y-Nd-0.8Ag present the large and deep crack with a certain extent corrosion product peeling off from surface. The magnesium alloy is

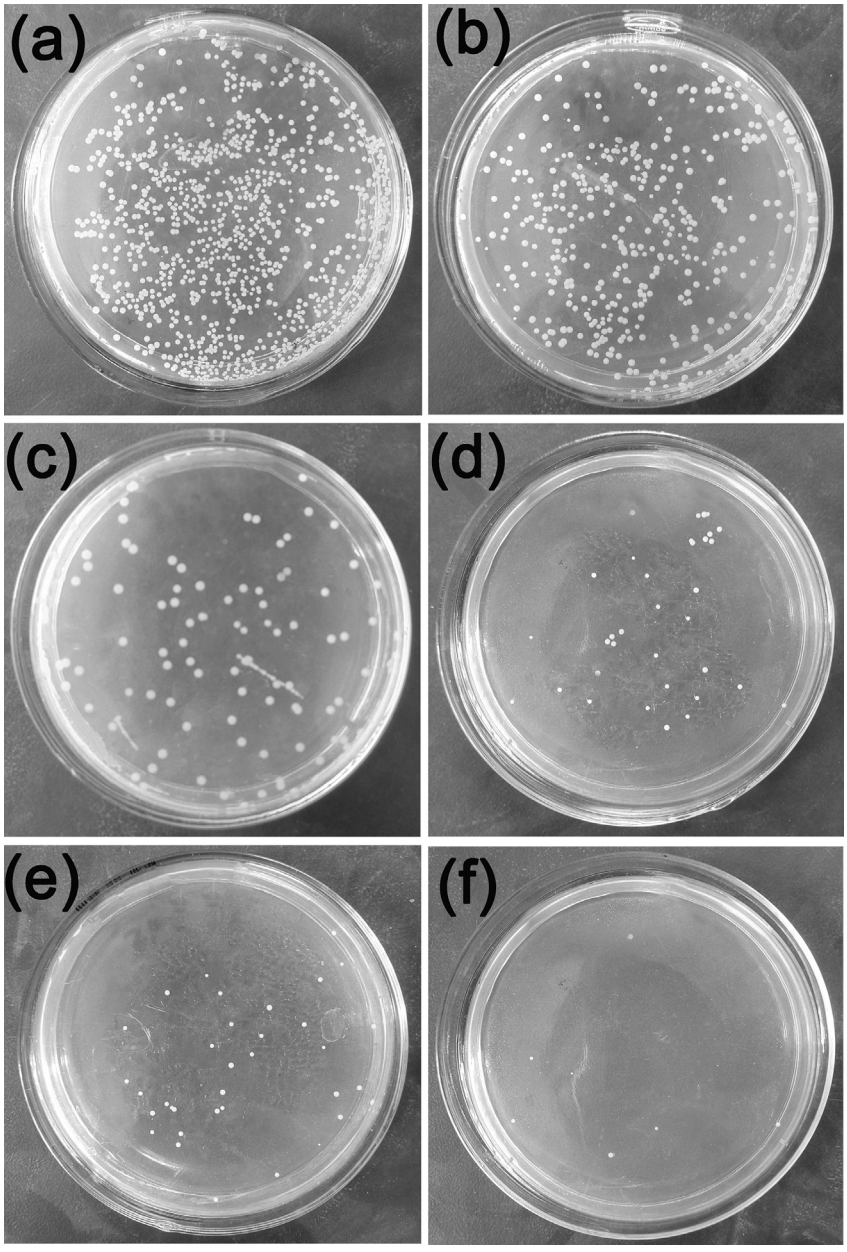

Fig. 10.

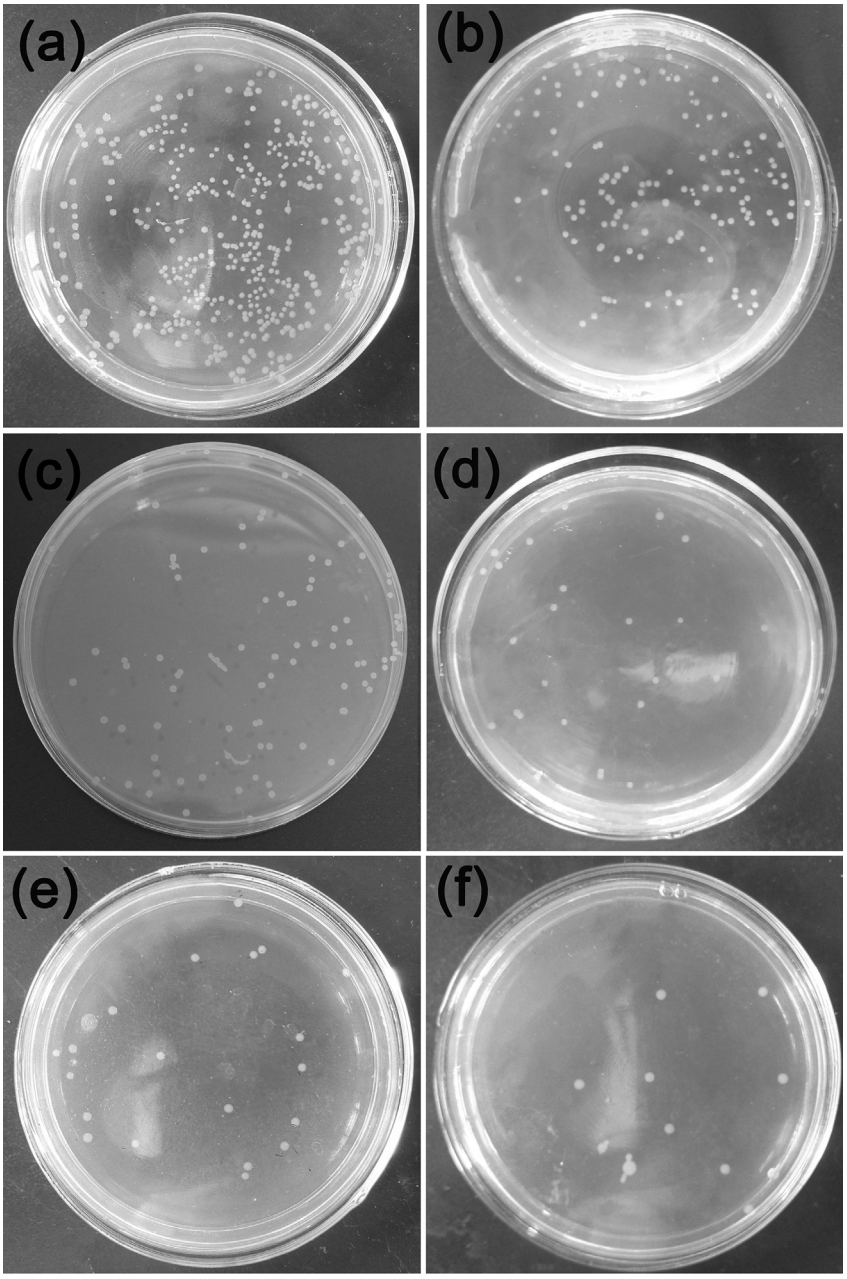

Fig. 11.

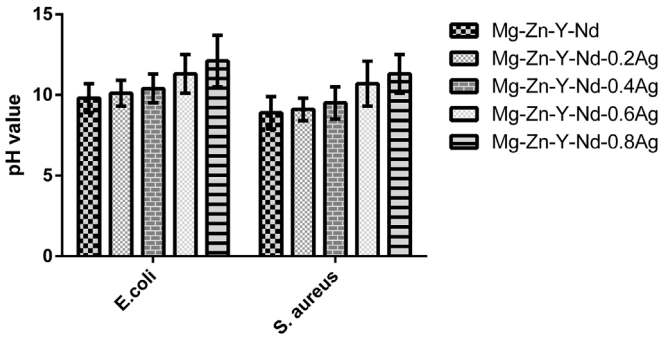

Fig. 12.

dominated by pitting corrosion, the more Ag content being added in the matrix, the more serious the pitting corrosion tendency is [17]. The different corrosion potential between the second phase and matrix of alloy generated a galvanic cell to accelerate the corrosion rate of matrix rounding the second phase. Corrosion pit points extended along the vertical and horizontal directions with the gradually extension of immersion time and ultimately give rise to matrix peeled off. Besides, as is shown in the Fig. 9, bright grains were appeared on the surface of the all Mg-Zn-Y-Nd-xAg alloys, which suggests the high silver content in the EDS result. The bright grains may be the corrosion products of silver. When the content of Ag exceeds the value of 0.4 wt%, corrosion products contain Ag element would gather into coarse dendrites. The antibacterial capability of alloys containing Ag element is mainly contributed to Ag ion [18]. From the immersion test, the Ag element indeed

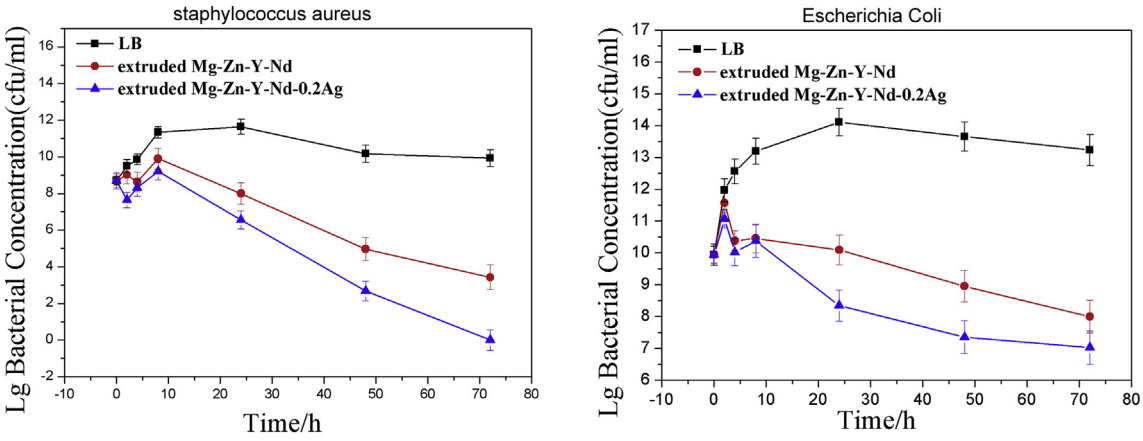

Fig. 13.

decomposes into ion form, which enables the antibacterial properties of alloy.

3.5. Antibacterial action on S. aureus and E. coli

Fig. 10 shows the bacterial form of *Escherichia Coli* by co-culture with extruded Mg-Zn-Y-Nd-xAg alloys after 24 h. From the figure, it is found that the highest bacterial concentration appears at co-culture with broth medium, which is higher than that treated by co-culture with Mg-Zn-Y-Nd-Ag alloys for 24 h. There is a decreasing trend of bacterial concentration of the *Escherichia Coli* with the Ag content increases. Also, it is found that the Mg-Zn-Y-N alloys exhibit certain antibacterial property. In the process of the co-culture experiment, the pH of the agar was increased in the meanwhile owing to the plenty of OH^- produced by the corrosion of Mg alloys, which means the pH of the agar environment would not be suitable for the growth and proliferation of the bacteria. The pH values of the bacteria solution co-cultured with Mg-Zn-Y-Nd-xAg for 24 h was shown in Fig. 12. Similarly, antibacterial property of the Mg-Zn-Y-Nd-xAg toward *staphylococcus aureus* is enhanced with the increment of silver content, and yet, Mg-Zn-Y-Nd-0.4Ag has already shown a good antibacterial property (Fig. 11).

It is indicated by the electrochemical experiment and hydrogen evolution test that the corrosion resistance of the alloys was gradually decreased with the increase of Ag content. As the result of the corrosion resistance decreased, the pH of culture medium was increased more rapidly during the immersion, which adversely influenced the growth and proliferation of the bacteria. To eliminate the influence of pH factor that originated by different corrosion resistance on the experiment results as much as possible, a 72-h antibacterial test was conducted with the alloys of Mg-Zn-Y-Nd and Mg-Zn-Y-Nd-0.2Ag, which were in possession of similar corrosion resistance (Fig. 12). The results indicated that the microbial concentration of extruded Mg-Zn-Y-Nd-0.2Ag alloys is higher than two order of magnitude as compared with Mg-Zn-Y-Nd, which suggests the more excellent antibacterial property. These are attributed to the action of Ag. The antibacterial mechanism of Ag^+ containing materials is not yet fully understood. It is generally considered that Ag^+ ion released from Ag^+ containing material plays a very important role. Cowan et al. [23] reported that the dose of Ag^+ ions has antimicrobial function. However, the Ag concentration may be reduced by some ionic in the bacterial suspension, such as Cl^- ions, since silver chloride are low soluble salt in the bacterial suspension [24,25] It is well known that Ag ions and Ag-based materials can strongly destroy the cell walls and cell membranes of bacteria to inhibit their breeding [26,27]. The references show that except for the silver ions, the second phase particle containing silver also plays an important role in antibacterial properties. Ag compounds particles can directly interact with membrane proteins of bacteria, accumulating in the cell membrane and affecting membrane permeability [28,29]. However, in our study, there was no second phase containing Ag detected, thus the Ag ions may have the major impacts on the antimicrobial property. The higher the silver content of the alloys, the relatively lower corrosion resistance and the more the silver ion generated by degradation. In addition to the formation of indissolvable substance with some ions in the bacteria solution, part of silver ions also plays an important role in sterilization. Silver ions in antibacterial material active oxygen to produce hydroxy and O^{2-}, and bacterial metabolic disturbance might inhibit or kill bacteria owning to the DNA molecular damaged by O^{2-} [19,20] (see Fig. 13).

4. Conclusion

In the present study, as-cast and as-extruded Mg-Zn-Y-Nd-XAg alloys with different concentrations of Ag (0.2, 0.4, 0.6 and 0.8%) were investigated in aspects of the microstructure, mechanical properties, corrosion behavior and antibacterial activities. It was found that the mechanical properties of as-cast Mg-Zn-Y-Nd-xAg alloys were improved with the addition of Ag element and the implementation of extrusion process, which significant enhanced the mechanical properties. The results of the electrochemical test and hydrogen evolution experiment indicate that the corrosion resistance of Mg-Zn-Y-Nd-XAg alloy was decreased with the increase of Ag contents, which mainly resulted from the formation of microgalvanic cell between α-Mg and the new phase (Ag51Nd14). However, after extrusion process, the corrosion resistance of the alloys was improved in certain degree. Mg-Zn-Y-Nd-xAg alloys exhibited effective antibacterial function both on *S. aureus* and *E. coli* according to the antibacterial effect assay. In conclusion, the Mg-Zn-Y-Nd-0.4Ag present the most excellent comprehensive performance, which indicates the promising potentiality of the alloy in clinical as an orthopedic implant.

Acknowledgement

We are grateful for the financial support of the National High-tech Research and Development Projects (863) (2015AA033603, 2015AA020301), the National Key Research and Development Program of China (2016YFC1102403) and the Major Science and Technology Projects in Henan Province (141100310900).

References

[1] J. Niu, M. Xiong, X. Guan, J. Zhang, The in vivo degradation and bone-implant interface of Mg-Nd-Zn-Zr alloy screws: 18 months post-operation results, Corros. Sci. 113 (2016) 183–187.

[2] T.A. Grünewald, H. Rennhofer, B. Hesse, M. Burghammer, S.E. Stanzl-Tschegg, M. Cotte, J.F. Lffler, A.M. Weinberg, H.C. Lichtenegger, Magnesium from bioresorbable implants: distribution and impact on the nano- and mineral structure of bone, Biomaterials 76 (2016) 250–260.

[3] J. Wang, L.M. Liu, Y.F. Wu, M.F. Maitz, Z.H. Wang, Y.M. Koo, A.S. Zhao, J. Sankar, D.L. Kong, N. Huang, Y. Yun, Ex vivo blood vessel bioreactor for analysis of the biodegradation of magnesium stent models with and without vessel wall integration, Acta Biomater. 50 (2017) 546–555.

[4] Y.S. Feng, S.J. Zhu, L.G. Wang, L. Chang, B.B. Yan, X.Z. Song, S.K. Guan, Characterization and corrosion property of nano-rod-like HA on fluoride coating supported on Mg-Zn-Ca alloy, Bio. Mater. 2 (2017) 63–70.

[5] S. Wei, Q. Zhao, Influence of reducers on nanostructure and surface energy of silver coatings and bacterial adhesion, Surf. Coat. Technol. 204 (2016) 1288–1294.

[6] Y. Li, L. Liu, P. Wan, Z. Zhai, Z. Mao, Z. Ouyang, D. Yu, Q. Sun, L. Tan, L. Ren, Z. Zhu, Y. Hao, X. Qu, K. Yang, K. Dai, Biodegradable Mg-Cu alloy implants with antibacterial activity for the treatment of osteomyelitis: in vitro and in vivo evaluations, Biomaterials 106 (2016) 250–263.

[7] H.R. Bakhsheshi-Rad, E. Hamzah, H.T. Low, M. Kasiri-Asgarani, S. Farahany, E. Akbari, M.H. Cho, Fabrication of biodegradable Zn-Al-Mg alloy:Mechanical properties, corrosion behavior, cytotoxicity and antibacterial activities, Mater. Sci. Eng. C Mater. 73 (2017) 215–219.

[8] H. Qin, Y.C. Zhao, Z.Q. An, M.Q. Cheng, Q. Wang, T. Cheng, Q.J. Wang, J.X. Wang, Y. Jiang, Xianlong Zhang, Guangyin Yuan, Enhanced antibacterial properties, biocompatibility, and corrosion resistance of degradable Mg-Nd-Zn-Zr alloy, Biomaterials 53 (2015) 211–220.

[9] H.Q. Tang, T. Liu, X. Liu, H.Q. Gu, J. Zhao, A study on biocompatibility and bactericidal properties of pyrolytic carbon by silver ion implantation, Nucl. Instrum. Meth. Phys. Res. B 255 (2007) 304–308.

[10] W. Shao, X. Liu, H. Min, G. Dong, Q. Feng, Preparation, characterization, and antibacterial activity of silver nanoparticle-decorated graphene oxide nanocomposite, ACS Appl. Mater. Interfaces 12 (2015) 6966–6973.

[11] C.F. Huang, H.J. Chiang, W.C. Lan, H.H. Chou, K.L. Ou, Development of silver-containing austenite antibacterial stainless steels for biomedical applications Part I: microstructure characteristics, mechanical properties and antibacterial mechanisms, Biofouling 27 (2011) 449–457.

[12] Y.F. Zheng, B.B. Zhang, B.L. Wang, Y.B. Wang, L. Li, Q.B. Yang, L.S. Cui, Introduction of antibacterial function into biomedical TiNi shape memory alloy by the addition of element Ag, Acta Biomater. 7 (2011) 2758–2767.

[13] Q. Wu, S. Zhu, L. Wang, Q. Liu, G. Yue, The microstructure and properties of cyclic extrusion compression treated Mg-Zn-Y-Nd alloy for vascular stent application, J. Mech. Behav. Biomed. Mater. 8 (2012) 1.

[14] T. Kokubo, H. Takadama, How useful is SBF in predicting in vivo bone bioactivity, Biomaterials 27 (2006) 2907–2915.

[15] C.Z. Zhang, S.J. Zhu, L.G. Wang, R.M. Guo, G.C. Yue, Microstructures and degradation mechanism in simulated body fluid of biomedical Mg–Zn–Ca alloy processed by high pressure torsion, Mater. Des. 96 (2016) 54–62.

[16] Y.M. Zhu, A.J. Morton, J.F. Nie, Improvement in the age-hardening response of Mg–Y–Zn alloys by Ag additions, Scr. Mater. 58 (2008) 525–528.

[17] D. Tie, F. Feyerabend, N. Hort, D. Hoeche, K.U. Kainer, R. Willumeit, W.D. Mueller, In vitro mechanical and corrosion properties of biodegradable Mg–Ag alloys, Mater. Corros. 65 (2014) 569–576.

[18] R. Kumar, H. Münstedt, Silver ion release from antimicrobial polyamide/silver composites, Biomaterials 26 (2005) 2081–2088.

[19] M. Rai, A. Yadav, A. Gade, Silver nanoparticles as a new generation of antimicrobials, Biotechnol. Adv. 27 (2009) 76–83.

[20] S.Y. Chen, M.T. Huang, S. Pender, M. Ruslin, H.H. Chou, K.L. Ou, The application of silver nano-particles on developing potential treatment for chronic rhinosinusitis: antibacterial action and cytotoxicity effect on human nasal epithelial cell model, Mater. Sci. Eng. C 80 (2017) 624–630.

[21] P. Mwaanga, E.R. Carraway, P. van den Hurk, The induction of bio-chemical changes in Daphnia magna by CuO and ZnO nanoparticles, Aquat. Toxicol. 150 (2014) 201–209.

[22] T.S. Lim, H.S. Ryu, S.H. Hong, Electrochemical corrosion properties of CeO2-containing coatings on AZ31 magnesium alloys prepared by plasma electrolytic oxidation, Corros. Sci. 62 (2012) 104–111.

[23] M.M. Cowan, K.Z. Abshire, S.L. Houk, S.M. Evans, Antimicrobial efficacy of a silver-zeolite matrix coating on stainless steel, J. Ind. Microbiol. Biotechnol. 30 (2003) 102–106.

[24] Y. Zheng, B. Zhang, B. Wang, Y. Wang, L. Li, Q. Yang, L. Cui, Introduction of antibacterial function into biomedical TiNi shape memory alloy by the addition of element Ag, Acta Biomater. 7 (2011) 2758–2767.

[25] A. Ewald, S.K. Glückermann, R. Thull, U. Gbureck, Antimicrobial titanium/silver PVD coatings on titanium, Biomed. Eng. 5 (2006) 22.

[26] H. Cao, X. Liu, F. Meng, P.K. Chu, Biological actions of silver nanoparticles embedded in titanium controlled by micro-galvanic effects, Biomaterials 32 (2011) 693–705.

[27] H. Cao, Y. Qiao, X. Liu, T. Lu, T. Cui, F. Meng, P.K. Chu, Electron storage mediated dark antibacterial action of bound silver nanoparticles: smaller is not always better, Acta Biomater. 9 (2013) 5100–5110.

[28] M. Chen, E. Zhang, L. Zhang, Microstructure, mechanical properties, biocorrosion properties and antibacterial properties of Ti–Ag sintered alloys, Mater. Sci. Eng. C 62 (2016) 350–360.

[29] H. Qin, H. Cao, Y. Zhao, C. Zhu, T. Cheng, Q. Wang, X. Peng, M. Cheng, J. Wang, G. Jin, Y. Jiang, X. Zhang, X. Liu, P.K. Chu, In vitro and in vivo anti-biofilm effects of silver nanoparticles immobilized on titanium, Biomaterials 35 (2014) 9114–9125.